The Journal of Chemical Physics | ARTICLE | scitation.org/journal/jcp

Long-range correlation of intra-molecular and inter-molecular vibration in liquid CCl_4

Cite as: J. Chem. Phys. 154, 034502 (2021); doi: 10.1063/5.0036091
Submitted: 2 November 2020 • Accepted: 29 December 2020 •
Published Online: 19 January 2021

David P. Shelton[a)]

AFFILIATIONS

Department of Physics and Astronomy, University of Nevada, Las Vegas, Nevada 89154-4002, USA

[a)]Author to whom correspondence should be addressed: shelton@physics.unlv.edu

ABSTRACT

Experiments measuring the polarization dependence of hyper-Raman light scattering reveal long-range correlation of molecular vibrations in liquid CCl_4. The ν_3 and $\nu_1 + \nu_4$ intra-molecular vibrations at about 770 cm^{-1} are strongly polarized transverse to the scattering wavevector. Weaker transverse polarization is exhibited by the ν_1, ν_2, and ν_4 intra-molecular vibrations and by the inter-molecular collision-induced band around 0 cm^{-1}. The observed polarization dependence is due to the correlation of the vibrations on molecules separated by about 200 nm. The strength of the observed correlation increases with the transition dipole moment for the vibration mode and is consistent with dipole–dipole coupling.

I. INTRODUCTION

The long-range correlation of the atomic position and motion in crystals is predominantly the result of strong short range interactions between the atoms. The same short range attractive and repulsive interactions may be present in liquids, but in liquids, they do not produce the long-range order seen in crystalline solids. For times short compared to the structural relaxation time, liquids are structurally similar to amorphous solids and glasses, with a fixed configuration of neighbors around each molecule.[1] Normal modes for such disordered media are a mixture of localized modes and non-local diffusive and propagating modes.[2–6] The normal modes of the inter- and intra-molecular vibrations for the instantaneous configuration in a liquid are collective but may be local, and as the inter-molecular interaction strength decreases, the intra-molecular vibrations become more strongly localized on individual molecules. Carbon tetrachloride is considered to be a liquid with weak inter-molecular interactions, where one expects the intra-molecular vibrations to be localized on individual molecules. Contrary to this expectation, based on hyper-Raman scattering (HRS) measurements, one finds that there is long-range correlation of the molecular vibrations in CCl_4 due to the long-range dipole–dipole interaction.

The propagating phonons in crystals have transverse or longitudinal polarization with respect to the wavevector of the phonon, and such transverse and longitudinal vibration modes can be identified by combining results from infrared and Raman spectra or from the polarization dependence of hyper-Raman spectra. Earlier HRS studies of crystals, glasses, and liquids found evidence for transverse and longitudinal nonlocal vibration modes in several molecular liquids including CCl_4.[7,8] Recently, there have been several more HRS studies of glasses and liquids[9–13] and liquid CCl_4, in particular.[12,13] The observations in the more recent studies are consistent with the earlier work but were not interpreted in terms of nonlocal vibration modes.

Long-range correlation of molecular orientation has been observed using hyper-Rayleigh scattering measurements in a number of liquids,[14] with extensive measurements for water,[15] nitrobenzene,[16] acetonitrile, and dimethyl sulfoxide.[17] Hyper-Rayleigh scattering is hyper-Raman scattering centered at zero frequency shift mediated by the molecular first hyperpolarizability tensor β, and these hyper-Rayleigh scattering measurements have been interpreted in terms of long-range molecular orientation correlation due to dipole–dipole coupling.[18–21] The orientation pair correlation function for the dipolar (first rank irreducible spherical tensor) part of β for the molecules in the liquid must vary as r^{-3} at long range to produce the observed transverse HRS.[19,20] The effect of correlation on hyper-Raman scattering, mediated by the transition hyperpolarizability, is similar.

The present work applies the HRS measurement techniques and analysis used in the study of long-range orientation correlation in liquids to the study of vibration correlation in liquid CCl_4. Local modes and nonlocal transverse and longitudinal modes are distinguished by the polarization dependence of HRS for the mode.[22,23] The HRS scattering configurations with incident and scattered light polarized either perpendicular or parallel to the horizontal scattering plane are denoted VV, HV, VH, and HH, where V denotes vertical polarization, H denotes horizontal polarization, and the first and second letters refer to the incident and scattered light, respectively. At 90° scattering angle, the HRS intensity ratio I_{HV}/I_{VH} for a polar vibration mode is I_{HV}/I_{VH} = 1, 2, or 0 according to whether the mode is local, transverse, or longitudinal. The experimental study below presents HRS spectral measurements for liquid CCl_4 in four linear polarization configurations. The measurements are combined to decompose the spectrum into local, transverse, and longitudinal components, and the results are interpreted in terms of a dipole–dipole correlation model.

II. EXPERIMENT

The experiment measures scattered light that is Raman-shifted from the laser second harmonic frequency. Linearly polarized pulses from an injection-seeded, cavity-dumped, single longitudinal mode Nd:YAG (yttrium aluminum garnet) laser (operating at $\lambda = 1064$ nm, 10 kHz repetition rate, 6 ns pulse duration, and 100 MHz line width) are focused to a 8 μm diameter beam waist in the liquid sample in a standard square 10 mm fluorimeter cuvette. The average laser power was about 2 W, and the peak intensity at the focus was about 2/3 of the 340 GW/cm^2 intrinsic laser induced breakdown threshold for CCl_4. To avoid breakdown at the focus, dust was removed from the CCl_4 sample by continuous flow in a closed loop containing the sample cell and a 0.2 μm PTFE (polytetrafluoroethylene) filter. Scattered light at $\theta = 90°$ was collected and collimated by using an aspheric lens (f = 4 mm), analyzed by using a linear polarizer, focused into an optical fiber, and fiber-coupled to the spectrometer and photon counting detector.

A scanning grating spectrometer was used to measure the HRS spectrum and also to measure the HRS intensity at selected fixed frequencies. The spectral slit width was 12 cm^{-1} [full width at half maximum (FWHM)] for all the HRS measurements. Multiple scans were averaged to eliminate the effect of 2% laser power fluctuation and drift during the measurements, and the spectra are corrected for the spectral response of the system. Spectra for polarization analysis were acquired from sequential scans of the spectrum with VV, HH, VH, and HV polarization. This sequence was repeated about 3000 times, and the spectra were summed for each polarization configuration.

The spectrometer response has strong polarization dependence, so an effective depolarizer is required between the analyzing polarizer and the spectrometer. The combination of a long multimode fiber (18 m) followed by a liquid crystal polymer microarray depolarizer was used. The polarization response of the system was calibrated using a thermal light source and integrating sphere placed at the sample position.

The HRS intensity ratios I_{VV}/I_{HV}, I_{HV}/I_{VH}, and I_{HH}/I_{VH} at each fixed frequency selected by the spectrometer were accurately measured using techniques previously described.[24] Several hundred alternate 10 s measurements of the two polarization configurations for each ratio are averaged to cancel the effect of intensity fluctuation and drift. Rapid switching between polarization configurations was done using a liquid crystal variable wave plate (LCVWP) to control the laser polarization and a fast rotator to control the analyzing polarizer for the scattered light.

The collection numerical aperture (NA) was controlled by a circular aperture following the collection lens. The HRS intensity ratio at NA = 0 was obtained by extrapolating measurements in the range 0.12 < NA < 0.50 to zero collection aperture. The accuracy of the polarization ratio NA extrapolation and the scattering angle setting were tested using measurements of Mie scattering at $\lambda = 532$ nm from a suspension of 85 nm diameter polystyrene microspheres in H_2O (40 ppm by weight, intrinsic depolarization ratio $= 3.2 \times 10^{-3}$) in the same apparatus.[25] Except for the VV HRS survey spectrum with NA = 0.50, spectra were scanned with NA = 0.12 and corrected for the effect of the finite collection aperture (corrections <1%). The HRS photon count rate varied from 2000 s^{-1} for the most intense peak (0 cm^{-1}, VV, NA = 0.5) to 0.1 s^{-1} for the weakest peak (216 cm^{-1}, VH, NA = 0.12). The background count rate of the gated photomultiplier was 0.0011 s^{-1}. The CCl_4 HRS signal showed no deviation from quadratic power dependence, and the sample temperature was 25 °C for all measurements.

III. EXPERIMENTAL RESULTS

The VV HRS spectrum measured for CCl_4 is shown in Fig. 1, and the HRS peak parameters obtained from the fit to the data are given in Table I. Details of the fitted curves are given in the supplementary material. The peak ν_0 is the rotational and collision-induced HRS spectrum,[26] ν_1 is the symmetric stretch vibration, ν_2 is the scissor mode, ν_4 is the bending mode, and ν_3 is the asymmetric stretch, which is in Fermi resonance with the $\nu_1 + \nu_4$ combination band.[12,27]

HRS polarization ratios measured for each peak are given in Table II. The ratio $I_{HH}/I_{VH} = 1.000 \pm 0.005$ was measured at $\nu = 760$ cm^{-1}, $I_{HH}/I_{VH} = 1.001 \pm 0.001$ was previously measured at $\nu = 0$ cm^{-1},[14] and $I_{HH}/I_{VH} = 1$ is assumed in the following analysis. At scattering angle $\theta = 90°$ and assuming Kleinman symmetry, the HRS intensities due to the octupolar contribution A_0, the dipolar transverse mode contribution A_T, and the dipolar longitudinal mode contribution A_L are[22,23]

$$I_{VV} = (3/2)A_0 + 9A_T, \tag{1}$$

$$I_{HV} = A_0 + A_T, \tag{2}$$

$$I_{HH} = I_{VH} = A_0 + (1/2)(A_T + A_L), \tag{3}$$

where $I_{VV}/I_{HV} = 3/2$ for pure octupolar HRS (third rank irreducible spherical tensor part of β) and $I_{VV}/I_{HV} = 9$ for pure dipolar HRS (first rank irreducible spherical tensor part of β).[7,10,28]

The HRS intensities measured with VV, HV, and VH linear polarization configurations are combined to determine the octupolar mode, polar transverse mode, and polar longitudinal mode contributions using the following relations:

$$A_0 = (6/5)I_{HV} - (2/15)I_{VV}, \tag{4}$$

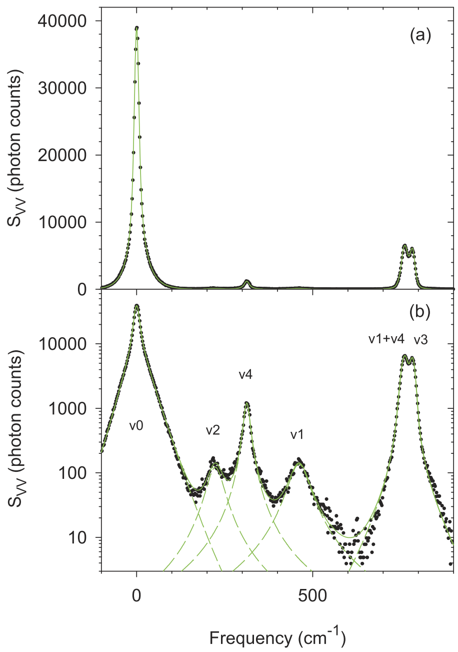

FIG. 1. VV HRS spectrum of CCl_4 scanned with 12 cm^{-1} spectral resolution, plotted with (a) linear and (b) logarithmic intensity scale. The solid curve fit to the data points is the sum of the contributions for each peak (dashed curves). Frequency ν is the Stokes Raman shift.

$$A_T = (2/15)I_{VV} - (1/5)I_{HV}, \tag{5}$$

$$A_L = (2/15)I_{VV} - (11/5)I_{HV} + 2I_{VH}. \tag{6}$$

The relative size of the dipolar and octupolar HRS contributions determined from the measured intensity ratio I_{VV}/I_{HV} is shown as the ratio A_T/A_0 in Table II. The ν_0 peak at $\nu = 0$ cm^{-1} is predominantly octupolar HRS, the ν_3 and $\nu_1 + \nu_4$ peaks are predominantly dipolar HRS, and the other peaks have comparable octupolar and dipolar contributions.

Nonlocal polar mode contributions are determined from the measured HRS intensity ratio I_{HV}/I_{VH} and are indicated by the ratio A_L/A_T in Table II. Local modes produce $A_L/A_T = 1$, so the deviation from $A_L/A_T = 1$ indicates a nonlocal polar mode contribution.

TABLE I. Peak positions, widths (FWHM), and normalized integrated intensities for the VV HRS spectrum in Fig. 1.

Mode	ν_p (cm^{-1})	$2\Delta\nu$ (cm^{-1})	Intensity
$\nu_0(A_1)$	0	20 ± 1	1000
$\nu_2(E)$	223 ± 2	47 ± 2	7 ± 1
$\nu_4(F_2)$	312 ± 1	19 ± 1	28 ± 1
$\nu_1(A_1)$	461 ± 1	57 ± 1	9 ± 1
$\nu_1 + \nu_4(F_2)$	762 ± 1	22 ± 1	135 ± 1
$\nu_3(F_2)$	784 ± 1	17 ± 1	86 ± 1

All the modes in Table II show a significant nonlocal mode contribution. The ν_3 and $\nu_1 + \nu_4$ modes with $A_L/A_T = 0$ are almost pure transverse polar modes.

The two most intense bands in the HRS spectrum have been studied in more detail. Figure 2 shows the HRS spectra with VV, HV, VH, and HH polarization for the Fermi resonance doublet at about 770 cm^{-1}, and Fig. 3 shows the VV, HV, VH, and HH spectra for the hyper-Rayleigh band centered at 0 cm^{-1}. There is no significant observed deviation from $I_{HH}/I_{VH} = 1$ for either band, so the spectral intensity data have been analyzed using Eqs. (4)–(6) to obtain the octupolar, transverse dipolar, and longitudinal dipolar spectra.

Figure 2(b) shows that the polarization ratios over the central part of the 770 cm^{-1} band are $I_{VV}/I_{HV} \approx 8$ and $I_{HV}/I_{VH} \approx 1.8$, indicating a dominant transverse polar nonlocal mode. Both polarization ratios decrease in the wings of the spectrum, indicating an additional broader local octupolar contribution. This is confirmed in Figs. 2(c) and 2(d), which show the octupolar, transverse dipolar, and longitudinal dipolar spectral components obtained from the spectra in Fig. 2(a) using Eqs. (4)–(6).

The A_T spectrum in Fig. 2(c) is fit by the sum of two peaks, each of which is the convolution of a Gaussian and an exponentially clipped Lorentzian function. A Lorentzian function decreases too slowly in the wings, so it is multiplied by a symmetric exponentially decreasing function to better represent the observed spectrum. The Gaussian function represents the spectrometer transmission function and other spectral broadening contributions. Simpler functions are adequate to fit the A_0 and A_L spectra in Fig. 2(d). The A_0 spectrum is fit by the sum of two exponentially clipped Lorentzians with the same peak positions as the peaks in the A_T spectrum, and the A_L spectrum is fit by the sum of two equal-width Gaussian functions. Details of the fit functions are given in the supplementary material.

TABLE II. HRS polarization ratios for CCl_4 measured at frequency shift ν with 12 cm^{-1} spectral resolution at 90° scattering angle and extrapolated to zero collection aperture.

Mode	ν (cm^{-1})	I_{VV}/I_{HV}	I_{HV}/I_{VH}	A_T/A_0	A_L/A_0	A_L/A_T
ν_0	0	1.872 ± 0.018	1.010 ± 0.004	0.052 ± 0.003	0.031 ± 0.009	0.60 ± 0.16
ν_2	216	3.89 ± 0.14	1.072 ± 0.025	0.47 ± 0.04	0.27 ± 0.07	0.58 ± 0.14
ν_4	313	6.71 ± 0.22	1.028 ± 0.012	2.28 ± 0.31	2.10 ± 0.31	0.92 ± 0.03
ν_1	461	3.86 ± 0.13	1.034 ± 0.024	0.46 ± 0.04	0.36 ± 0.07	0.79 ± 0.14
$\nu_1 + \nu_4$	762	8.37 ± 0.05	1.847 ± 0.011	11.0 ± 0.9	−0.01 ± 0.11	−0.001 ± 0.010
ν_3	784	8.20 ± 0.05	1.800 ± 0.011	8.35 ± 0.60	0.04 ± 0.09	0.005 ± 0.011

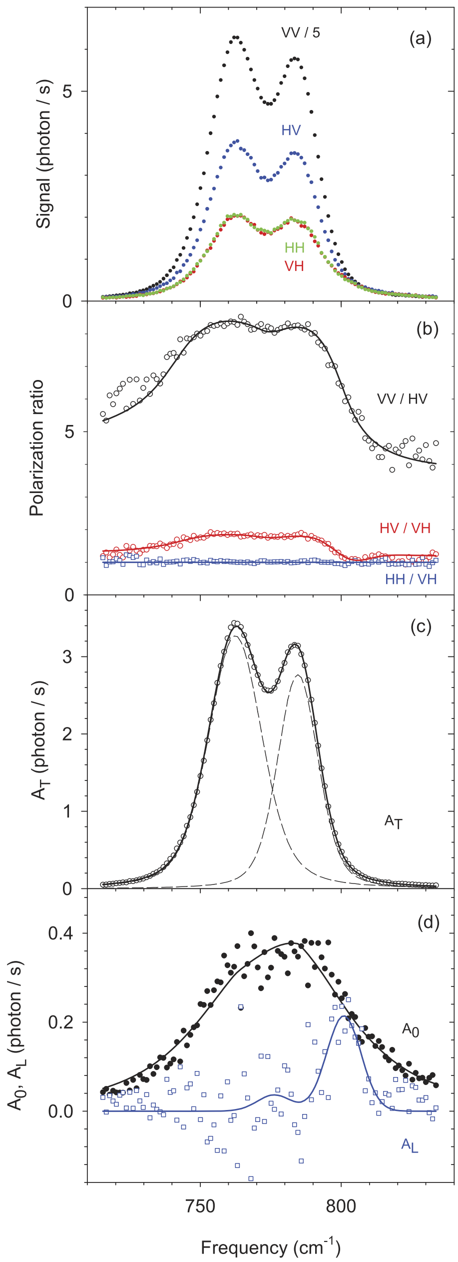

FIG. 2. (a) HRS spectra for the ν_3 and $\nu_1 + \nu_4$ modes, showing data points measured with four linear polarization configurations. Data points obtained by combining the data at each frequency are shown for the (b) polarization ratios, (c) intensity A_T, and (d) intensities A_0 and A_L. The function fit to the combined data is shown by the solid curves, with the separate ν_3 and $\nu_1 + \nu_4$ components shown by the dashed curves in (c).

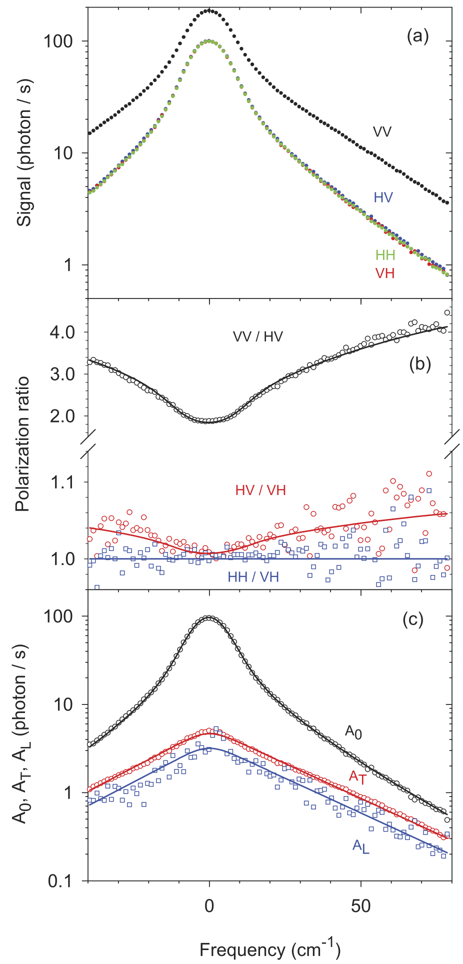

FIG. 3. (a) HRS spectra for the ν_0 mode, showing data points measured with four linear polarization configurations. Data points obtained by combining the data at each frequency are shown for (b) the polarization ratios and (c) the intensities A_0 and A_T and A_L. The function fit to the combined data is shown by the solid curves.

The separation of the $\nu_1 + \nu_4$ and ν_3 peaks is 22.3 ± 0.2 cm^{-1} for the A_T spectrum and 25 ± 5 cm^{-1} for the A_L spectrum, not significantly different, but the peaks in the A_L spectrum are shifted up from the A_T peaks by 16 ± 2 cm^{-1}. The frequency difference between the longitudinal and transverse spectral peaks can be estimated using the Lyddane–Sachs–Teller relation $\nu_L/\nu_T = (\epsilon_0/\epsilon_\infty)^{1/2}$ for the LO and TO mode frequencies of dipolar modes.[29,30] For CCl_4 where $\epsilon_0 = 2.2379$ and $\epsilon_\infty \approx n^2 = (1.46)^2 = 2.13$, this relation gives $\nu_L/\nu_T = 1.025$ and an LO–TO splitting of 19 cm^{-1}, close to the observed splitting. The longitudinal spectrum is much weaker than the transverse spectrum. The ratio of integrated intensities for the A_L and A_T peaks is 0.006 ± 0.004 for $\nu_1 + \nu_4$ and 0.060 ± 0.007 for ν_3.

The analysis of the hyper-Rayleigh spectra in Fig. 3 is similar to that previously reported.[26] The octupolar A_0 spectrum in Fig. 3(c) is fit by the sum of a narrow exponentially clipped Lorentzian and a broader exponential component, multiplied by the exponential Boltzmann factor and convolved with a Gaussian. The Lorentzian is the rotational HRS spectrum, and the broad exponential is the collision-induced spectrum. The dipolar collision-induced A_T spectrum is fit by a broad exponential function multiplied by the exponential Boltzmann factor and convolved with the same Gaussian.

The A_L spectrum is fit by the scaled A_T spectrum, with intensity ratio A_L/A_T = 0.683 ± 0.014. The fit functions are given in the supplementary material.

IV. DISCUSSION

The HRS observations in Fig. 2 indicate the presence of long-range correlation of the molecular vibrations in liquid CCl_4. The polarized HRS spectra for the ν_3 and $\nu_1 + \nu_4$ vibrations in liquid CCl_4 are similar to HRS spectra for TO and LO propagating phonon modes in a crystal,[7] except that for the liquid, the longitudinal mode contribution is much weaker than the transverse mode contribution. Similar polarization dependence, with a dominant transverse mode contribution, has been observed for hyper-Rayleigh scattering from polar liquids such as water[15] and acetonitrile[17] due to long-range molecular orientation correlation.

The long-range orientation correlation in water[18] is due to the permanent dipole moment $\mu_0 = 6.2 \times 10^{-30}$ Cm for H_2O.[31] A possible mechanism for vibration correlation in CCl_4 is resonant dipole–dipole coupling between the transition dipole moments on vibrating molecules, analogous to the dipole–dipole coupling between permanent molecular dipoles. The transition dipoles for the CCl_4 fundamental vibrations are $\mu = 7.75 \times 10^{-31}$ Cm for ν_3 and 3.09×10^{-32} Cm for ν_4,[32] much smaller than typical permanent dipoles. However, alignment of the transition dipole may be facilitated because the dipole produced by a linear combination of the three-fold degenerate modes for an F_2 symmetry vibration is free to point in any direction.

A simple model for long-range vibration correlation in CCl_4 is given by the correlation tensor for a solenoidal vector field with r^{-3} asymptotic dependence.[19,20] The components of the diagonal correlation tensor, longitudinal and transverse to the inter-molecular vector $\mathbf{r}$, are

$$B_L(r) = [1 + (r/a)^2]^{-3/2}, \tag{7}$$

$$B_T(r) = [1 + (r/a)^2]^{-3/2}[1 - (3/2)r^2/(r^2 + a^2)]. \tag{8}$$

These functions are shown in Fig. 4(a) and can also be expressed in terms of rotational invariants $\Phi^{110} = \hat{\mu}_1 \cdot \hat{\mu}_2$ and $\Phi^{112} = 3(\hat{\mu}_1 \cdot \hat{r})(\hat{\mu}_2 \cdot \hat{r}) - \hat{\mu}_1 \cdot \hat{\mu}_2$, with coefficients $h^{110} = B_L + 2B_T$ and $h^{112} = 2B_L - 2B_T$, where $\hat{\mu}_1$ and $\hat{\mu}_2$ are the transition dipole unit vectors for molecules 1 and 2.[33,34] The Fourier transform of this correlation tensor gives the spectral intensities transverse and longitudinal to the scattering wavevector $\mathbf{K}$,

$$S_T(Ka \ll 1) = 2\pi a^3, \tag{9}$$

$$S_L(K) = 0. \tag{10}$$

A more realistic correlation function is obtained by modifying Eqs. (7) and (8) with an excluded volume, which gives $B_L(r) = B_T(r) = 0$ for $r < r_1$, and adding a delta-function self-correlation at $r = 0$ with volume integral $\rho^{-1}/3$, where $\rho^{-1} = 4\pi r_0^3/3$ is the volume per molecule. The spectral intensities with this modified correlation function, for $Ka \ll 1$, are[20]

$$S_T = 2\pi a^3 + 4\pi r_0^3/9 - (4\pi a^3/3)[1 + (a/r_1)^2]^{-3/2}, \tag{11}$$

$$S_L = 4\pi r_0^3/9 - (4\pi a^3/3)[1 + (a/r_1)^2]^{-3/2}. \tag{12}$$

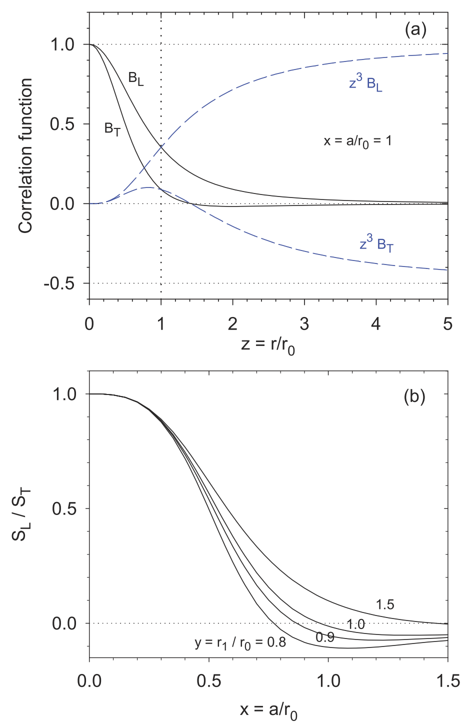

FIG. 4. (a) Model correlation functions, B_L and B_T from Eqs. (7) and (8) for $a = r_0$, with asymptotic limits shown by horizontal dotted lines. (b) Longitudinal/transverse intensity ratios for modified correlation functions with $B_L = B_T = 0$ for $0 < r < r_1$. The intermolecular separation $z = r/r_0$, the cutoff radius for the correlation function $y = r_1/r_0$, and the correlation strength $x = a/r_0$ are scaled by the molecular radius r_0.

The difference between S_T and S_L is entirely due to the correlation at a long range, $r > K^{-1} = \Lambda/2\pi$.[18] Figure 4 of Ref. 18 showed the Fourier transform integrals [Eqs. (19) and (20) of Ref. 18] for S_T and S_L plotted as functions of the upper integration limit r_2 for the correlation functions given in Eqs. (7) and (8). For small r_2, the difference $S_T - S_L = 0$, but $S_T - S_L$ begins to increase for $r_2 > 0.5\ K^{-1}$, and $S_T - S_L$ reaches its asymptotic value for $r_2 > 10\ K^{-1}$. The main contribution to the difference $S_T - S_L$ is from $r_2 \approx 5\ K^{-1}$, for correlation lengths close to the wavelength Λ of the scattering wavevector. For CCl_4 in these experiments, K^{-1} = 41 nm, and the main contribution to $S_T - S_L$ is from correlation at $r \approx 200$ nm.

The parameter a in Eqs. (11) and (12) is a measure of the strength of long-range correlation with r^{-3} asymptotic dependence. The value for a may be determined from a fit to experimental values for S_T and S_L, but the result obtained for a from this fit will have some dependence on the assumed form of the short range correlation. A more accurate result for a could be obtained using a more accurate short range vibration correlation function from a molecular dynamics simulation, similar to the calculation of the orientation correlation functions for the analysis of hyper-Rayleigh scattering.[16–18] The spatial intensity spectra $S_L(K)$ and $S_T(K)$ produced by the most general correlation function for a homogeneous isotropic random vector field are given by the Fourier transform expressions [Eqs. (11) and (12) of Ref. 19].

Figure 4(b) shows S_L/S_T determined from Eqs. (11) and (12), plotted vs normalized correlation strength $x = a/r_0$ for several values of the normalized cutoff radius $y = r_1/r_0$. The un-physical negative values for S_L/S_T obtained for correlation parameter $a > r_1$ are due to the abrupt cutoff at r_1. A normalized cutoff radius $y = 0.88$ for CCl_4 is obtained from the liquid density of 6.24 nm^{-3} and the Lennard-Jones diameter of 0.59 nm.[31,35] The analysis of previous HRS experiments found a cutoff at $y = 1.04$ for water[18] and $y = 0.90$ for nitrobenzene,[16] and the dipole orientation correlation strength is $x = 0.86$ for water[18] and $x = 0.58$ for nitrobenzene.[16] In that work, the short range part of the orientation correlation function was determined from a molecular dynamics simulation.

The observed ratio $S_L/S_T = A_L/A_T = 0.060 \pm 0.007$ for the ν_3 mode in CCl_4 is obtained from Fig. 4(b) for $x = 0.79$ and $y = 0.90$, and the observed ratio $A_L/A_T = 0.006 \pm 0.004$ for the $\nu_1 + \nu_4$ mode is obtained for $x = 0.85$ and $y = 0.90$. The long-range vibration correlation for these modes in CCl_4 is comparable to the long-range orientation correlation $x = 0.86$ for water.

The correlation strength varies as $a^3 \propto \mu^2$ for dipole–dipole coupling. Since the transition dipole for the ν_4 mode is 25 times smaller than for ν_3, one expects much weaker long-range correlation for ν_4 than for ν_3. If $a/r_0 = 0.79$ for ν_3, then $a/r_0 = 0.09$ is estimated for ν_4, and Fig. 4(b) gives $S_L/S_T = 0.997$ for the ν_4 mode as compared to $A_L/A_T = 0.92 \pm 0.03$ that is observed.

The ratios $A_L/A_T \neq 1$ measured for the ν_0, ν_2, and ν_1 modes indicate the presence of long-range correlation for these modes, even though their symmetry species are non-dipolar. However, the molecules are distorted by interactions with neighbor molecules. The electric field of the octupole moment on one CCl_4 molecule induces a dipole on its neighbor during close collisions, and the dipole–dipole interaction can produce orientation correlation between the collision-induced dipoles on widely separated molecules, similar to the orientation correlation between molecules with permanent dipoles seen in hyper-Rayleigh scattering from dipolar liquids.[14–17]

The average squared field $\langle E^2 \rangle$ at distance r from a CCl_4 molecule is

$$\langle E^2 \rangle = (48/5)(4\pi\epsilon_0)^{-2}\Omega_{xyz}^2/\langle r^{-10} \rangle, \tag{13}$$

where Ω_{xyz} is the only independent nonzero component of the octupole moment tensor for CCl_4. The field $E = 4.9 \times 10^8$ V/m, calculated using Eq. (13) and the parameter values in Table III, will induce a dipole $\mu = \alpha_0 E = 6.1 \times 10^{-31}$ Cm on a colliding neighbor molecule. The induced dipole is parallel to the field E since the polarizability tensor is isotropic. This induced dipole is about the same size as the transition dipole for the ν_3 mode, so the degree of orientation correlation for the collision-induced dipoles is expected to be comparable to the correlation observed for the ν_3 vibration. The collision trajectories for widely separated pairs of colliding molecules must be correlated by the dipole–dipole interaction to produce this orientation correlation of the induced dipoles.

The molecular octupole field also induces a contribution $\Delta\beta = \gamma E$ on each colliding neighbor molecule. The magnitude of induced $\Delta\beta = 3.8 \times 10^{-52}$ C^3 m^3 J^{-2} is comparable to permanent β_{xyz}, and a previous study found that $\Delta\beta$ makes a large contribution to the HRS signal.[26] The tensor γ for CCl_4 is nearly isotropic, differing from a sphere only in that $\gamma_{zzzz} = \gamma_{zzxx} + \gamma_{zxzx} + \gamma_{zxxz}$ may not hold. The induced $\Delta\beta$ due to the isotropic part of γ transforms as a vector aligned with the induced dipole, so it has the same orientation correlation as the dipole, and transverse polarized HRS is expected as a result.

TABLE III. Molecular parameters for CCl_4, where α_0 is the static polarizability, β and γ are from gas phase measurements at $\lambda = 1064$ nm, Ω is from gas phase far-IR absorption, ϵ and σ are for the Lennard-Jones 6–12 potential, ρ is the liquid density, and $\rho^{-1} = 4\pi r_0^3/3$.

Parameter	Value	Reference
α_0	1.25×10^{-39} C^{2}m^{2}J^{-1}	36
β_{xyz}	$5.4 \pm 0.4 \times 10^{-52}$ C^{3}m^{3}J^{-2}	37
$\langle\gamma\rangle_{zzzz}$	$7.7 \pm 0.1 \times 10^{-61}$ C^{4}m^{4}J^{-3}	38
Ω_{xyz}	$5.3 \pm 1.0 \times 10^{-49}$ Cm^3	39
ϵ/k_B	327 K	35
σ	0.588 nm	35
r_0	0.337 nm	
ρ	6.24×10^{27} m^{-3}	31
$\langle r^{-6}\rangle$	2.6×10^{56} m^{-6}	26
$\langle r^{-10}\rangle$	1.1×10^{93} m^{-10}	26

Long-range polar orientation correlation of collision-induced dipolar $\Delta\beta$ can account for $A_L/A_T < 1$ that is observed for the ν_0, ν_1, ν_2, and ν_4 modes, which have a small or zero transition dipole. For the ν_0 mode, uncorrelated random orientational diffusion of β produces the Lorentzian octupolar spectrum in Fig. 3(c), fluctuating short range orientation correlation of β produces the exponential wing of the octupolar spectrum in Fig. 3(c), while modulation of $\Delta\beta$ during a collision produces the exponential dipolar spectrum in Fig. 3(c).[26] From Fig. 4(b) using the value $S_L/S_T = A_L/A_T = 0.60 \pm 0.16$ that is observed in Fig. 3(c), one estimates correlation strength $x = a/r_0 = 0.47$ for the dipolar inter-molecular contribution to the ν_0 mode.

HRS from the E symmetry species ν_2 mode is forbidden by symmetry (but not exactly when the T_d symmetry is lowered by isotope effects), so most of the HRS signal is due to the collision-induced contribution modulated at the ν_2 vibration frequency. Vibrational modulation of $\Delta\beta$ can occur through the dependence of Ω_{xyz} and $\langle\gamma\rangle$ on the vibrational coordinate. Long-range orientation correlation with $x = a/r_0 = 0.48$ for the dipolar collision-induced $\Delta\beta$ can account for $A_L/A_T = 0.58 \pm 0.14$ that is observed for the ν_2 mode.

HRS from the A_1 symmetry ν_1 mode will have an allowed octupolar contribution and a collision-induced contribution from $\Delta\beta$ modulated at the ν_1 vibration frequency. One expects the same correlation for the dipolar collision-induced $\Delta\beta$ for ν_0, ν_1, and ν_2 modes, but the observed result $A_L/A_T = 0.79 \pm 0.14$ for ν_1 indicates a weaker correlation. However, the ν_1 band is overlapped by the $2\nu_2$ overtone band, which has an allowed dipolar β contribution but a transition dipole too small to produce significant vibration correlation. The uncorrelated $2\nu_2$ contribution added to the ν_1 collision-induced $\Delta\beta$ contribution results in a reduced average correlation and increased A_L/A_T, so dipolar collision-induced $\Delta\beta$ with correlation $x = a/r_0 > 0.37$ can account for the ν_1 observations.

The ν_4 mode has both allowed and collision-induced HRS contributions. The observed $A_L/A_T = 0.92 \pm 0.03$ is due to the combination of a contribution with correlation $x = a/r_0 > 0.26$ from dipolar collision-induced $\Delta\beta$ modulated at the ν_4 vibration frequency, diluted by the allowed HRS contribution for which the small ν_4 transition dipole results in negligible vibration correlation.

Effects of vibration correlation are also seen in other experiments. Transition dipole coupling in polar molecular liquids produces the frequency shifts observed in the spectral non-coincidence effect, where the frequencies of the infrared, isotropic Raman, and anisotropic Raman components of a polar vibration band do not coincide.[40–42] The effect is seen when the orientation of permanent molecular dipoles is correlated by dipole–dipole (or hydrogen bond) interactions between the polar molecules, and the symmetry axis for the IR active stretching vibration is aligned with the permanent dipole of the polar molecule. The frequency shift due to vibration transition dipole correlation is a function of $\Phi^{110} = \hat{\mu_1} \cdot \hat{\mu_2}$, so it is not sensitive to long-range correlation due to dipole–dipole coupling.

Theory for the coupling of transition dipoles associated with infrared-active vibrations has been developed for crystals,[43] and it has been extended and applied to calculate the LO–TO splitting produced by dipole coupling in ionic liquids.[44] Transition dipole-transition dipole coupled vibration is also observed in the Raman spectrum of liquid and plastic crystal CF_4, where the split ν_3 peak is assigned as LO and TO modes.[45,46] Recent molecular dynamics simulations and normal mode analysis of ice find both highly localized and de-localized vibration modes,[47] and recent molecular dynamics calculations for liquid water find propagating phonon-like modes with a LO–TO splitting, indicating the presence of coherent long-range dipole–dipole interactions.[48]

HRS measurements are uniquely sensitive to long-range correlation of polar modes in isotropic media.[19,20,22,23] Previous HRS experiments that observed LO and TO modes for liquid CCl_4 emphasized the phonon-like character of the vibrations,[7,8] but the modes in disordered dense media may be de-localized and non-propagating. The present experiments are consistent with long-range vibration correlation with r^{-3} dependence. This spatial dependence could be tested with measurements of polarization dependent HRS as a function of scattering angle.[15–17]

V. CONCLUSION

The polarization dependence of hyper-Raman scattering from liquid CCl_4 provides evidence for long-range correlation of the molecular vibrations in the liquid for both the intra-molecular vibration modes and the inter-molecular modes (collision-induced HRS). Direct coupling between the transition dipoles can account for the correlation for dipolar vibration modes with a large transition dipole. The transient dipole and aligned vector hyperpolarizability induced during molecular collisions can account for the vibration correlations for modes with small or zero transition dipole. The observations are consistent with a correlation function that has r^{-3} asymptotic dependence, and the correlation strength parameter is estimated from the HRS measurements.

SUPPLEMENTARY MATERIAL

See the supplementary material for spectral curve fit data.

ACKNOWLEDGMENTS

This work was supported by the National Science Foundation under Award No. CHE-1953941.

DATA AVAILABILITY

The data that support the findings of this study are available within this article.

REFERENCES

[1] K. Trachenko and V. V. Brazhkin, Rep. Prog. Phys. **79**, 016502 (2016).
[2] H. R. Seyf, L. Yates, T. L. Bougher, S. Graham, B. A. Cola, T. Detchprohm, M.-H. Ji, J. Kim, R. Dupuis, W. Lv, and A. Henry, npj Comput. Mater. **3**, 49 (2017).
[3] Y. M. Beltukov, C. Fusco, A. Tanguy, and D. A. Parshin, J. Phys.: Conf. Ser. **661**, 012056 (2015).
[4] P. B. Allen, J. L. Feldman, J. Fabian, and F. Wooten, Philos. Mag. B **79**, 1715 (1999).
[5] R. Orbach, J. Non-Cryst. Solids **164-166**, 917 (1993).
[6] B.-C. Huang and C.-H. Chang, Phys. Rev. E **88**, 042116 (2013).
[7] V. N. Denisov, B. N. Mavrin, and V. B. Podobedov, Phys. Rep. **151**, 1 (1987).
[8] V. N. Denisov, B. N. Mavrin, V. B. Podobedov, and K. E. Sterin, Sov. Phys. JETP **57**, 733 (1983).
[9] B. Hehlen and G. Simon, J. Raman Spectrosc. **43**, 1941 (2012).
[10] V. Rodriguez, J. Raman Spectrosc. **43**, 627 (2012).
[11] V. Rodriguez, J. Grondin, F. Adamietz, and Y. Danten, J. Phys. Chem. B **114**, 15057 (2010).
[12] G. Guimbretière, A. Bouchet, V. Rodriguez, M. Couzi, D. Talaga, T. Buffeteau, and L. Canioni, J. Phys. Chem. C **112**, 17906 (2008).
[13] O. Quinet, B. Champagne, and V. Rodriguez, J. Chem. Phys. **121**, 4705 (2004).
[14] D. P. Shelton, J. Chem. Phys. **136**, 044503 (2012).
[15] D. P. Shelton, J. Chem. Phys. **141**, 224506 (2014).
[16] D. P. Shelton, J. Chem. Phys. **144**, 234506 (2016).
[17] M. B. Rodriquez and D. P. Shelton, J. Chem. Phys. **148**, 134504 (2018).
[18] D. P. Shelton, J. Chem. Phys. **147**, 154501 (2017).
[19] D. P. Shelton, J. Chem. Phys. **143**, 134503 (2015).
[20] D. P. Shelton, J. Chem. Phys. **146**, 199901 (2017).
[21] D. P. Shelton, J. Chem. Phys. **138**, 154502 (2013).
[22] D. P. Shelton, J. Opt. Soc. Am. B **17**, 2032 (2000).
[23] D. P. Shelton, J. Opt. Soc. Am. B **34**, 1550 (2017).
[24] D. P. Shelton, Rev. Sci. Instrum. **82**, 113103 (2011).
[25] G. S. He, H.-Y. Qin, and Q. Zheng, J. Appl. Phys. **105**, 023110 (2009).
[26] P. Kaatz and D. P. Shelton, Mol. Phys. **88**, 683 (1996).
[27] T. Chakraborty and A. L. Verma, Spectrochim. Acta A **58**, 1013 (2002).
[28] P. D. Maker, Phys. Rev. A **1**, 923 (1970).
[29] C. Kittel, *Introduction to Solid State Physics* (Wiley, 1971).
[30] J. D. Hwang, T. K. Song, T. W. Noh, and S. I. Kwun, Phys. Rev. B **44**, 13067 (1991).
[31] R. C. Weast, *CRC Handbook of Chemistry and Physics*, 68th ed. (CRC, Boca Raton, 1987).
[32] D. M. Bishop and L. M. Cheung, J. Phys. Chem. Ref. Data **11**, 119 (1982).
[33] G. Stell, G. N. Patey, and J. S. Hoye, Adv. Chem. Phys. **48**, 183 (1981).
[34] J.-P. Hansen and I. R. McDonald, *Theory of Simple Liquids*, 4th ed. (Academic, 2013).
[35] J. O. Hirshfelder, C. F. Curtiss, and R. B. Bird, *Molecular Theory of Gases and Liquids* (Wiley, New York, 1954).

[36] M. P. Bogaard and B. J. Orr, in *International Review of Science, Physical Chemistry, Molecular structure and properties* (Butterworths, 1975), Ser. 2, Vol. 2, p. 149.
[37] D. P. Shelton, J. Chem. Phys. **137**, 044312 (2012).
[38] P. Kaatz, E. A. Donley, and D. P. Shelton, J. Chem. Phys. **108**, 849 (1998).
[39] I. R. Dagg, M. Missio, A. Anderson, W. Smith, and L. A. A. Read, Can. J. Phys. **67**, 507 (1989).
[40] D. E. Logan, Chem. Phys. **103**, 215 (1986).
[41] H. Torii and M. Tasumi, J. Chem. Phys. **99**, 8459 (1993).
[42] H. Torii, J. Phys. Chem. A **110**, 9469 (2006).
[43] J. C. Decius, J. Chem. Phys. **49**, 1387 (1968).
[44] C. M. Burba, Phys. Chem. Chem. Phys. **21**, 3976 (2019).
[45] M. Gilbert and M. Drifford, J. Chem. Phys. **66**, 3205 (1977).
[46] M. Yvinec and R. M. Pick, J. Chem. Phys. **71**, 3440 (1979).
[47] D. R. Moberg, S. C. Straight, C. Knight, and F. Paesani, J. Phys. Chem. Lett. **8**, 2579 (2017).
[48] D. C. Elton and M. Fernadez-Serra, Nat. Commun. **7**, 10193 (2016).